CONTROL OF NONLINEAR TUNE SHIFTS IN SLS 2.0

J. Avila Pulido*[1], J. Kallestrup
PSI Center for Accelerator Science and Engineering, 5232 Villigen PSI, Switzerland
[1] also at EPFL Laboratory of Particle Accelerator Physics, 1015 Lausanne, Switzerland

Abstract

The Swiss Light Source upgrade, SLS 2.0, is a next-generation storage ring featuring an ultra-low-emittance lattice based on a seven-bend achromat design. Achieving such low emittance requires strong focusing, which in turn generates large negative chromaticities. These are corrected using powerful sextupole magnets, introducing nonlinear effects in the beam dynamics. In particular, amplitude-dependent tune shifts (ADTS) and chromatic tune shifts (CTS) play a significant role. This contribution presents measurements of ADTS and CTS performed using high-precision tune measurements. Furthermore, since SLS 2.0 comprises 12 sectors equipped with 22 octupoles each, the control of ADTS and CTS through the use of octupoles is demonstrated.

INTRODUCTION

Ultra-low emittance lattices, such as the Swiss Light Source upgrade, SLS 2.0 [1], require strong focusing to achieve low emittance. However, this results in large negative natural chromaticities, which cause beam instabilities and beam loss. To compensate, strong sextupole magnets are used, but these introduce nonlinear beam motion, which can potentially reduce the dynamic aperture and beam lifetime. In particular, second-order effects such as amplitude-dependent tune shifts (ADTS) and second-order chromaticities become relevant. The ADTS (α_{ik}) and second-order chromaticities ($\xi_m^{(2)}$) are defined as

$$\alpha_{ik} = \frac{\partial Q_k}{\partial J_i}, \qquad \xi_m^{(2)} = \frac{\partial^2 Q_m}{\partial \delta^2}$$

with $i, k = x, y$ denote the horizontal and vertical planes, respectively, $Q_{x,y}$ the tunes, $J_{x,y}$ the actions. Also, $\alpha_{xy} = \alpha_{yx}$. δ denotes the energy deviation and $m = x, y$.

Each of the 12 arcs constituting the SLS 2.0 storage ring is equipped with 24 sextupoles and 22 octupoles used to control the nonlinear dynamics with the goal of maximizing dynamic aperture (DA) and Touschek lifetime (TL). Octupoles allow the control of ADTS and second-order chromaticities at first order [2], and therefore serve as efficient knobs for shaping the tune foot print to avoid resonance crossing [3–5]. Additionally, control of ADTS can be used in the context of round-beam operation while operating on the linear difference resonance, where horizontal off-axis injection will generally lead to unwanted vertical oscillations and occasionally beam losses. By tailoring the ADTS, it is possible to detune the injected beam away from the coupling resonance thereby avoiding losses [6–8].

* jesus.avila-pulido@psi.ch

Following [5], the knobs are defined in the following way,

$$\vec{A} = \mathbf{B}\vec{b}_4, \tag{1}$$

with $\vec{A} = (\alpha_{xx}, \alpha_{xy}, \alpha_{yy}, \xi_x^{(2)}, \xi_y^{(2)})^T$ and

$$\mathbf{B} = \begin{pmatrix} (\beta_x^2)_1 & \cdots & (\beta_x^2)_{N_{\text{oct}}} \\ -2(\beta_x\beta_y)_1 & \cdots & -2(\beta_x\beta_y)_{N_{\text{oct}}} \\ (\beta_y^2)_1 & \cdots & (\beta_y^2)_{N_{\text{oct}}} \\ 4(\eta^2\beta_x)_1 & \cdots & 4(\eta^2\beta_x)_{N_{\text{oct}}} \\ -4(\eta^2\beta_y)_1 & \cdots & -4(\eta^2\beta_y)_{N_{\text{oct}}} \end{pmatrix}, \tag{2}$$

with $\vec{b}_4$ containing the strengths of the N_{oct} octupoles. $\mathbf{B}$ is a $5 \times N_{\text{oct}}$ matrix with the values of the optical functions evaluated at the octupole locations.

In SLS 2.0, all 264 octupoles are independently powered. However, since measuring the changes in the second-order chromaticity and ADTS generated by individual octupoles is challenging, they were grouped into eight "families" according to the values of the optical functions at their locations: OXX, OXY and OYY (harmonic octupoles), and OCXM, OCY2, OCX2, OCY1, and OCX1 (chromatic octupoles). The current of each family can be varied independently in the range from -5 to 5 A, the equivalence in integrated octupole strength depends on the specific family.

It is worth noting that the optical functions are not exactly identical for all magnets within a given family in SLS 2.0. However, this approximation does not significantly affect the results.

The current octupole settings are a result of first a nonlinear optimization in simulation followed by a by-hand adjustment to achieve the best measured injection efficiency and lifetime.

SECOND-ORDER CHROMATICITY

To measure the second-order chromaticity, frequency shifts from -500 to 500 Hz in steps of 250 Hz were applied to the RF cavities. These shifts corresponds to energy deviations ranging from -1% to 1%. The tune in both planes was measured for each octupole setpoint using the mixed-BPM method with the Numerical Analysis of Fundamental Frequencies (NAFF) [9–11]. From the induced energy deviation, a second-order polynomial fit of Q as a function of δ was performed. The second-order chromaticity was extracted from this fit.

The measured second-order chromaticities in the horizontal and vertical planes are 4.21 ± 0.29 and 27.22 ± 0.28, respectively.

This procedure was repeated changing the strength of all octupoles in a given family in steps of $76\ \text{m}^{-3}$ (approximately

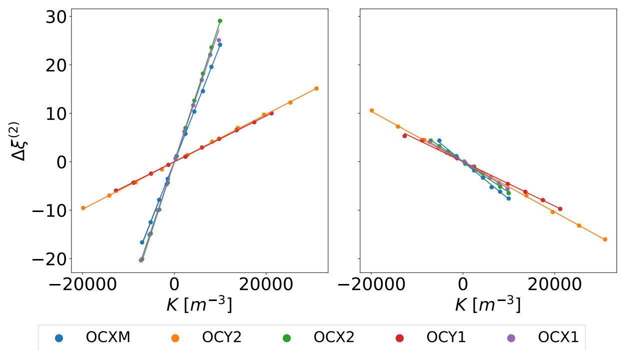

Figure 1: Change in second-order chromaticity as a function of octupole strength (K) for each family. The measured data points and the corresponding linear fits are shown. Left: horizontal plane. Right: vertical plane.

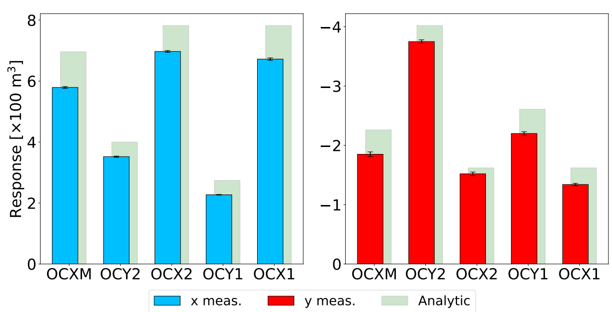

Figure 2: Response of the second-order chromaticity to variations in octupole strength for each family. The slopes extracted from Fig. 1 are compared with the analytical values from Eq. (2). Left: horizontal plane. Right: vertical plane.

1 A), in order to compare with the last two rows of Eq. (2). Since the coefficient of determination (R^2) for the second order fit exceeded 0.99 in all cases, a third order fit was unnecessary.

Figure 1 shows the results of this procedure. The response of the second-order chromaticity to changes in octupole strength is linear, as predicted by Eq. (1).

Figure 2 compares the slopes of the lines shown in Fig. 1 with the analytical values obtained from Eq. (2). In all cases, the measured values are lower than the analytical predictions; on average, they differ by about 10%. One possible source of this discrepancy is magnet calibration errors.

Figure 3 shows the maximum possible values that can be achieved using all families of octupoles.

An attempt was made to measure the second-order chromaticity using individual octupoles in order to compare the impact of local optics effects. However, the resulting $\Delta\xi^{(2)}$ values were so small that reliable measurements could only be obtained at the largest and smallest octupole strengths. Moreover, accurate determination of the chromatic shifts would require multiple measurements at each setpoint, as noticeable variations were observed between consecutive measurements. Given the large number of octupoles, this approach would result in a time-consuming procedure. Therefore, the measurements were performed by grouping the octupoles into families. Nevertheless, measuring $\Delta\xi^{(2)}$ for individual octupoles could be valuable for identifying potential magnet calibration errors.

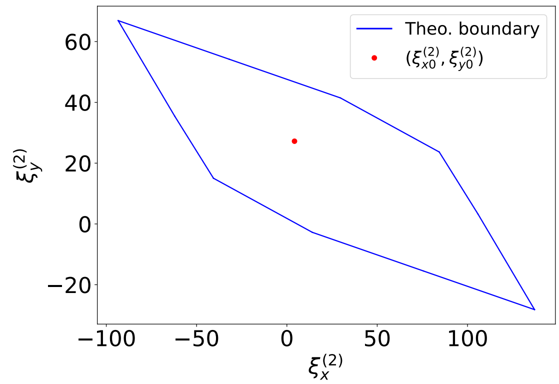

Figure 3: Possible values of the second-order chromaticity that can be achieved using all the octupole families. The maximum theoretical boundary and the initial second-order chromaticity are shown.

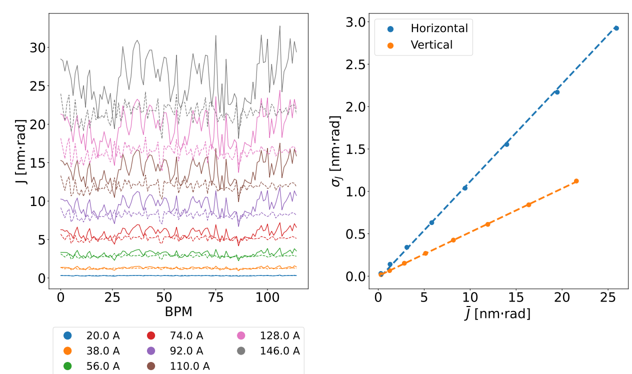

Figure 4: Left: Example of the measured J at each BPM. The solid and dashed lines correspond to J_x and J_y, respectively. Right: standard deviation of J as a function its average value.

AMPLITUDE DEPENDENT TUNE SHIFTS

To measure α_{xx} and α_{xy}, a horizontal pinger magnet was used to excite the beam. Its current was varied from 20 to 146 A in 8 steps. For each step, turn-by-turn (TbT) data over 2000 turns was acquired from 115 Beam Position Monitors (BPMs). Eleven samples were recorded and subsequently averaged. At the same time, a current of 10 A was applied to the vertical pinger magnet to provide a small excitation in the vertical plane.

For the measurement of α_{yy} and α_{yx}, the roles of the horizontal and vertical pingers were reversed. This procedure was repeated varying the strength of all octupoles within a given family in steps of 76 m^{-3}, in order to compare with the first three rows of Eq. (2).

To determine the ADTS coefficients, a linear fit of the tune as a function of the action was performed. The horizontal action was calculated from the maximum amplitude, $x_{\max}$, recorded by the BPMs according to: $J_x = \frac{x_{\max}^2}{2\beta_x}$, and similarly for the vertical plane.

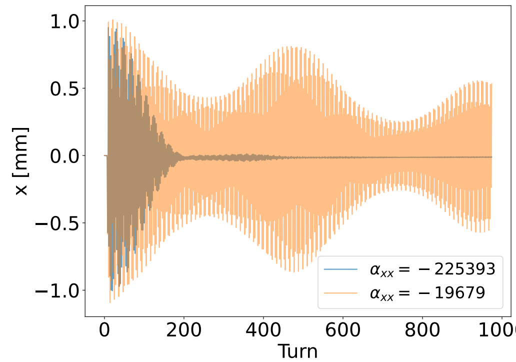

Figure 5: Turn-by-turn data recorded in a BPM for two different values of the ADTS.

Figure 4 shows a representative example of the measured action J at all BPMs. The standard deviation of J is observed to increase with the excitation current. This behavior can be attributed to BPM gain errors or optics errors. For this reason, the maximum excitation current considered in the analysis was limited to 146 A.

The tune was then determined using the NAFF method, considering only the first 60 turns. A limited number of turns was used due to decoherence effects arising from amplitude detuning. This is illustrated in Fig. 5, which shows TbT data for a case with a large and small α_{xx} but with the same chromaticity.

The linear fit of the tune as a function of J was performed independently for each BPM. The average slope was taken as the ADTS coefficient, and the standard deviation of the mean of the slopes was used as its uncertainty.

In the case of α_{xx} not all BPMs were used, as some of them recorded unrealistic tune variations. For α_{xy}, the tune measurement was noisy at low horizontal kicker currents. This can be attributed to the excitation amplitude being comparable to that produced by the vertical kicker (10 A). Therefore, only tune values corresponding to horizontal pinger currents above 74 A were retained.

For α_{yx}, since $\alpha_{xy} = \alpha_{yx}$ is expected, the tune should decrease with increasing kick strength as observed in α_{xy}. This behavior was used as a filtering criterion to select BPMs with a reliable signal.

The measured ADTS are $\alpha_{xx,0} = -62751 \pm 4545$, $\alpha_{yy,0} = 43960 \pm 2612$, and $\alpha_{xy,yx,0} = -55630 \pm 7124$, where the latter corresponds to the average of $\alpha_{xy,0}$ and $\alpha_{yx,0}$.

Figure 6 shows the change of the ADTS as a function of the change in octupole strength per family. As expected from Eq. (1), the relationship between the two variables is linear. Fig. 7 compares the slopes of the lines shown in Fig. 6 with the analytical values obtained from Eq. (2) showing good agreement.

It is important to note that the ADTS values and their response to variations in octupole strength are inversely proportional to the square of the BPM gains. This dependence arises because the maximum measured amplitude, which is required to determine the action, is equal to the true maximum amplitude multiplied by the gain of the corresponding

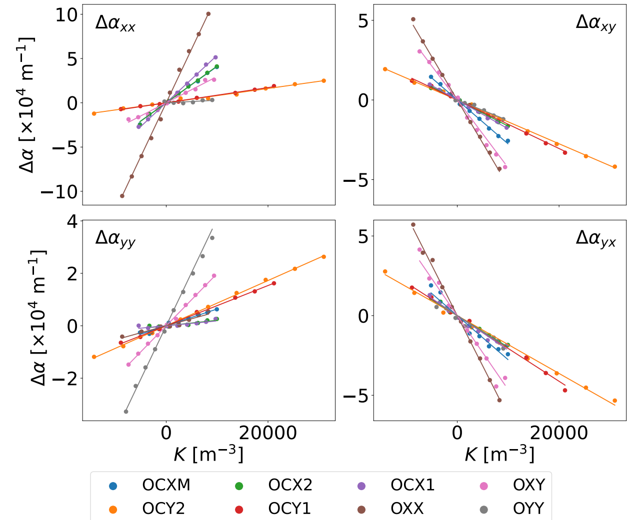

Figure 6: Changes in the ADTS as a function of the octupole strengths (K) per family.

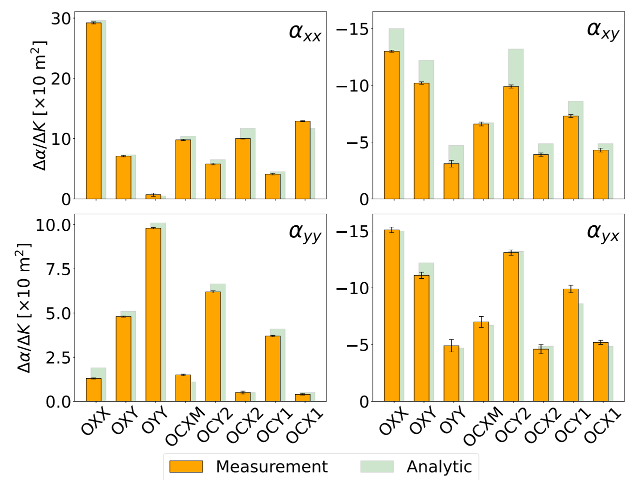

Figure 7: Response of the ADTS to changes in octupole strengths per family. The slopes of the lines in Fig. 6 are shown and compared with values obtained from Eq. (2).

BPM. In this study, all BPM gains were assumed to be equal to unity; therefore, any deviation from this assumption may affect the results.

The individual octupole families allow to modify α_{xx} from -22×10^4 to 2.5×10^4 m^{-1}, α_{xy} in the range from -9.5×10^4 to 2.5×10^4 m^{-1}, and α_{yy} from 0.5×10^4 to 7.5×10^4 m^{-1}. The octupole families can act together to further increase these intervals.

CONCLUSION

The response of the ADTS and the second-order chromaticity to variations in the octupole strengths was measured and compared with analytical predictions, showing good agreement. By using the octupoles as control knobs, different combinations of these parameters can be explored to optimize the beam lifetime and maximize the dynamic aperture of SLS 2.0.

REFERENCES

[1] A. Streun *et al.*, “Swiss light source upgrade lattice design”, *Phys. Rev. Accel. Beams*, vol. 26, p. 091601, 2023. doi:10.1103/PhysRevAccelBeams.26.091601

[2] M. Cornacchia and Y. Chin, “A study of the dynamic aperture limit in tristan”, *Part. Accel.*, vol. 17, pp. 191–213, 1985.

[3] L. Emery, “An Ultra-Low Emittance Damping Ring Lattice and Its Dynamic Aperture”, in *Proc. PAC’89*, Chicago, IL, USA, Mar. 1989, pp. 1225–1228.

[4] L. Emery, “Further Dynamic Aperture Studies on a Wiggler-based Ultra-low-emittance Damping Ring Lattice”, in *Proc. PAC’91*, San Francisco, CA, USA, May 1991, pp. 1633–1636.

[5] S. C. Leemann and A. Streun, “Perspectives for future light source lattices incorporating yet uncommon magnets”, *Phys. Rev. ST Accel. Beams*, vol. 14, p. 030701, 2011. doi:10.1103/PhysRevSTAB.14.030701

[6] M.-A. Tordeux *et al.*, “Injection Schemes for the SOLEIL Upgrade”, in *Proc. IPAC’21*, Campinas, Brazil, May 2021, pp. 796–798. doi:10.18429/JACoW-IPAC2021-MOPAB248

[7] T. Zhang and X. Huang, “Off-axis injection for storage rings with full coupling”, *Phys. Rev. Accel. Beams*, vol. 21, no. 8, p. 084002, Aug. 2018. doi:10.1103/PhysRevAccelBeams.21.084002

[8] M. Carlà, G. Benedetti, U. Iriso, Z. Martí, and L. Torino, “Methods for full coupling operation in a synchrotron light source”, *Phys. Rev. Accel. Beams*, vol. 28, no. 8, p. 082803, 2025. doi:10.1103/rhfy-8jsp

[9] J. Laskar, C. Froeschlé, and A. Celletti, “The measure of chaos by the numerical analysis of the fundamental frequencies. application to the standard mapping”, *Physica D: Nonlinear Phenomena*, vol. 56, no. 2, pp. 253–269, 1992. doi:10.1016/0167-2789(92)90028-L

[10] K. Paraschou, S. Kostoglou, and D. Pellegrini, Nafflib, https://github.com/PyCOMPLETE/NAFFlib

[11] P. Zisopoulos, Y. Papaphilippou, and J. Laskar, “Refined betatron tune measurements by mixing beam position data”, *Phys. Rev. Accel. Beams*, vol. 22, p. 071002, 2019. doi:10.1103/PhysRevAccelBeams.22.071002